

# ITER-like current ramps in JET with ILW: experiments, modelling and consequences for ITER

G.M.D. Hogewij<sup>1\*</sup>, G. Calabrò<sup>2</sup>, A.C.C. Sips<sup>3</sup>, C.F. Maggi<sup>4</sup>,  
G.M. De Tommasi<sup>5</sup>, E. Joffrin<sup>6</sup>, A. Loarte<sup>7</sup>, F. Maviglia<sup>5</sup>,  
J. Mlynar<sup>8</sup>, F.G. Rimini<sup>9</sup>, Th. Pütterich<sup>4</sup> and JET EFDA  
Contributors †

JET-EFDA, Culham Science Centre, Abingdon, OX14 3DB, UK

<sup>1</sup> FOM Institute DIFFER, Association EURATOM-FOM, Trilateral Euregio Cluster, P.O.Box 1207, Nieuwegein, The Netherlands, www.differ.nl

<sup>2</sup> Associazione Euratom-ENEA, Via Enrico Fermi 45, 0044 Frascati, Italy

<sup>3</sup> European Commission, Brussels, B-1049, Belgium

<sup>4</sup> Max-Planck-Institut für Plasmaphysik, Boltzmannstrasse 2, 85748 Garching, Germany

<sup>5</sup> Associazione EURATOM-ENEA-CREATE, Università di Napoli Federico II, 80125 Napoli, Italy

<sup>6</sup> Association Euratom-CEA, IRFM, F-13108 St-Paul-Lez-Durance, France

<sup>7</sup> ITER Organization, F-13115 St Paul Lez Durance, France

<sup>8</sup> Association EURATOM-IPP.CR, Prague, Czech Republic

<sup>9</sup> CCFE Fusion Association, Culham Science Centre, Abingdon OX14 3DB, UK

\*E-mail: g.m.d.hogewij@differ.nl

**Abstract.** Since the ITER-like wall in JET (JET-ILW) came into operation, dedicated ITER-like plasma current ( $I_p$ ) ramp-up (RU) and ramp-down (RD) experiments have been performed and matched to similar discharges with the carbon wall (JET-C). The experiments show that access to H-mode early in the  $I_p$  RU phase and maintaining H-mode in the  $I_p$  RD as long as possible are instrumental to achieve low internal plasma inductance ( $l_i$ ) and to minimize flux consumption. In JET-ILW, at a given current rise rate similar variations in  $l_i$  (0.7-0.9) are obtained as in JET-C. In most discharges no strong W accumulation is observed. However, in some low density cases during the early phase of the  $I_p$  RU ( $n_e/n_e^{Gw} \sim 0.2$ ) strong core radiation due to W influx led to hollow electron temperature ( $T_e$ ) profiles. In JET-ILW  $Z_{\text{eff}}$  is significantly lower than in JET-C. W significantly disturbs the discharge evolution when the W concentration approaches  $10^{-4}$ ; this threshold is confirmed by predictive transport modelling using the CRONOS code.  $I_p$  RD experiments in JET-ILW confirm the result of JET-C that sustained H-mode and elongation reduction are both instrumental in controlling  $l_i$ .

PACS numbers: 52.25.Fi, 52.55.Fa, 52.50.Gj

† See the Appendix of F. Romanelli et al., *Proceedings of 24th IAEA Fusion Energy Conference 2012, San Diego, USA*

## 1. Introduction

In the last years, simulations and experiments around the world have been focused on 15 MA scenarios for ITER [1], this being the most demanding of the ITER reference scenarios for the superconducting poloidal field (PF) coils. Indeed the PF system plays a crucial role during the plasma current ( $I_p$ ) ramp-up (RU) phase of a discharge: first, it must provide a stable plasma equilibrium during this phase; second, it must be able to provide the significant amount of magnetic flux that is needed to ramp up  $I_p$  inductively. Also the current ramp-down (RD) of a burning plasma is a challenging part of plasma operation. Apart from the issue of not exceeding the density limit, a burning plasma is usually in H-mode before the  $I_p$  RD and shall return to L-mode before termination. During the H-L transition the plasma quickly loses energy content, which needs to be properly handled by plasma shape, position and vertical stability systems.

The ITER PF coils must remain within several limits, such as coil current, coil field, voltage, power and central solenoid force limits. Allowing for control margins, the PF system of ITER will only allow a range of  $l_i = 0.7 - 1.0$  [2] (note that throughout this paper  $l_i$  refers to  $l_i(3)$ , as defined in e.g. [2]). Therefore it is important to perform ITER-like  $I_p$  RU and RD experiments in present-day tokamaks, and to extrapolate the results to ITER by predictive modelling. Such experiments have been done in most of the available large tokamaks, such as JET, ASDEX-U and DIII-D [2, 3, 4, 5]. Past JET experiments were done with a carbon wall (JET-C), so their results cannot directly be extrapolated to ITER. An all-metal ITER-like wall, consisting of beryllium (Be) in the main chamber and tungsten (W) surfaces in the divertor, has recently been installed in JET (JET-ILW) [6]. Therefore, dedicated ITER-like  $I_p$  RU and RD experiments have been set up in JET-ILW [7], and matched to similar discharges in JET-C [2, 3], in order to assess if the flux consumption and plasma inductance  $l_i$  evolution is modified by the Be-wall and W-divertor during the current rise and current decay: current profile evolution, plasma controllability issues such as W accumulation in the transient phase and L-H transition, and consequently to test predictive and interpretative transport modelling simulations. Flux consumption in this paper is always referring the total flux consumption, i.e. the sum of the resistive and inductive contribution. This paper also reports on interpretative and predictive modelling of the experimental results, performed with the CRONOS suite of codes [8], on the following issues:

- (i) the differences between C and Be as main intrinsic impurity, with respect to  $l_i$  evolution, flux consumption, electron temperature ( $T_e$ ), safety factor ( $q$ ) profile evolution and radiation;
- (ii) changes in  $l_i$  and flux consumption during  $I_p$  RU and RD, e.g. by early transition into H-mode and maintaining H-mode during  $I_p$  RD, and by reducing the elongation during the  $I_p$  RD;
- (iii) the maximum W concentration compatible with ohmic or heated  $I_p$  RU, without strongly perturbing  $l_i$  and  $T_e$  and  $q$  profiles.

In addition, predictive modelling of (iii) is performed for the  $I_p$  RU and RD phase of ITER, using the specifications given by the ITER team.

The paper is organized as follows: Section 2 describes the JET experimental conditions and the main observations in JET-ILW. Section 3 gives details on the transport models used for the simulations. Section 4 documents the differences and similarities between  $I_p$  RU in JET-C and JET-ILW. The possibilities for  $l_i$  control and flux consumption reduction in  $I_p$  RU and RD are discussed in section 5. Section 6 presents the role of W in the evolution of the plasma during JET-ILW  $I_p$  RU, both as observed in the experiment and as simulated by predictive modelling; this modelling has also been performed for ITER. Finally, in section 7 consequences for future ITER operation are discussed.

## 2. Experimental set-up and overview of results

The scenario used in the JET experiments was  $I_p = 2.5$  MA,  $B_t = 2.4$  T (corresponding to  $q_{95} \simeq 3$ ) at low triangularity  $\delta \simeq 0.25$ , low voltage break-down ( $E_{\text{axis}} \simeq 0.37$  V/m), early X-point formation at  $I_p = 0.8$  MA, with additional heating (NBI) applied from plasma current  $I_p = 1.5$  MA. This matches, using the plasma resistivity as guide, as discussed in [2], the proposed baseline inductive scenario for ITER of 15MA/5.3T ( $q_{95} \simeq 3$ ), X-point formation at  $\simeq 4$  MA and additional heating applied from  $I_p \simeq 9$  MA. This scenario was also used for previous JET-C ITER-like  $I_p$  RU studies [2, 3]. Experimental time traces of JET-ILW discharges with ITER-like  $I_p$  RU and their JET-C equivalents, are shown in Fig.1 for the ohmic case; the H-mode  $I_p$  RU will be shown in the next section (Fig.5). The following parameters were varied in the experiments:

- Input power: ohmic, low power L-mode (up to 2.8 MW ICRF) and H-mode (5 MW NBI) during the  $I_p$  RU and RD phases;
- Density: the Greenwald fraction  $n_e/n_e^{\text{Gw}}$  was varied from 0.2 to 0.4;
- $I_p$  ramp rate: the ramp-up rate used was  $dI_p/dt = 0.36, 0.28$  and  $0.19$  MA/s, to match the ITER  $I_p$  rise phases of 50s, 80s and 100s, respectively. The current ramp-down rate was varied between  $-0.14$  and  $-0.5$  MA/s along the same guidelines;
- Elongation during  $I_p$  RD was reduced from  $\kappa \simeq 1.68$  (typical value for JET shapes) to  $\simeq 1.54$  in a few pulses to control the  $l_i$  evolution.

The eXtreme Shape Controller (XSC) including the new Current Limit Avoidance (CLA) system was used from the X-point formation until the termination of the discharge in order to achieve good plasma shape control [9] during  $I_p$  RU and RD phases. The current L-H power threshold scaling law [10], used for extrapolations to ITER, predicts for D, in MW:

$$P_{\text{thr},08} = 0.049B_t^{0.80}n_{20}^{0.72}S^{0.94} \quad (1)$$

where  $B_t$  [T],  $n_{20}[10^{20}\text{m}^{-3}]$  and  $S$  [ $\text{m}^2$ ] are respectively the magnetic field, line-averaged density, and plasma surface area. Eq.(1) shows that the plasma surface area plays

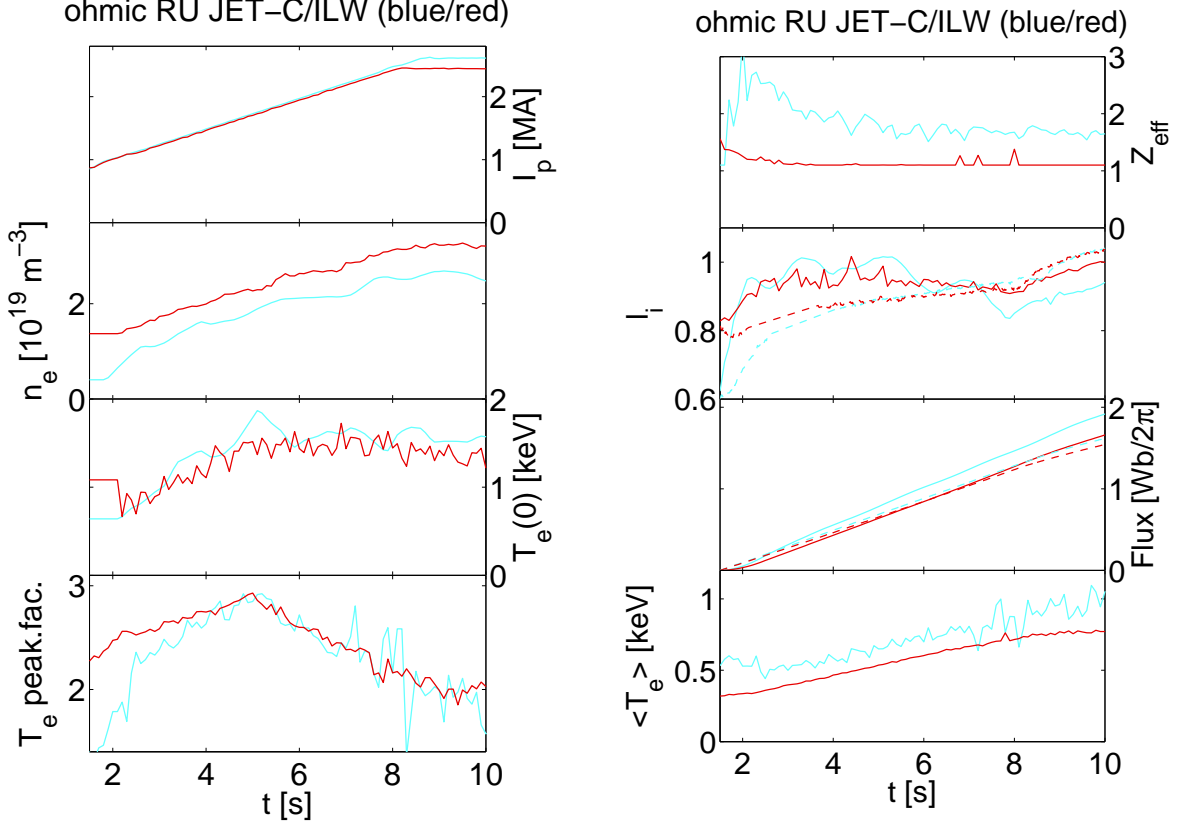


**Figure 1.** *Left:*  $I_p$ , line averaged  $n_e$ ,  $T_e(0)$  and  $T_e$  peaking for JET-C pulse 72723 (light cyan) and JET-ILW pulse 83223 (dark red), showing good match. *Right:*  $Z_{\text{eff}}$ ,  $l_i$ , total flux consumption and  $\langle T_e \rangle$  for the same pulses. Note: here and in following plots dashed lines are from interpretative modelling.

an important role in  $P_{\text{thr}}$ , hence that it is important to have a good control of the plasma shape whilst the plasma current is changing. Compared to the standard JET Shape Controller (SC, see also [9]), which has been used in the JET-C  $I_p$  RU and RD experiments before [2, 3], the XSC improves the plasma shape control, since it allows to control (in the least mean square sense) more than 30 plasma shape descriptors, whilst at most 4 plasma shape descriptors are controlled with SC. During the  $I_p$  RU phase the variation of the plasma surface is  $\sim 5\%$  with XSC, whilst it is  $\sim 10\%$  with SC. Furthermore, the XSC improves also the control of plasma shape during disturbances due to the poloidal  $\beta$  variation induced by the switch-on and switch-off of additional heating in current rise and decay [11].

As was found in [2, 3], the JET-ILW experiments showed that access to H-mode early in the ramp-up phase and maintaining H-mode in the ramp-down as long as possible are instrumental to achieve low internal plasma inductance  $l_i$  (0.7-0.8) and to minimize flux consumption. Table 1 lists pulse numbers,  $I_p$  ramp up rate, heating powers, electron density ( $n_e$ ), electron temperature ( $T_e$ ), effective charge of the plasma ( $Z_{\text{eff}}$ , derived from a single line-of-sight integral of the visible continuum emission) and  $l_i = l_i(3)$ , as defined in [2], and injected power for both JET-ILW and JET-C experiments; the quoted values are those obtained at the end of the  $I_p$  RU phase. Figure

2 summarizes the range of plasma inductance at the end of the current rise phase for JET-ILW and JET-C discharges compared to the ITER allowed range of  $l_i$ . In JET-ILW, at a given  $dI_p/dt$  similar variations in  $l_i$  (0.7-0.9) were obtained as in JET-C and are within the ITER margins; The only exception is the H-mode  $I_p$  RU at the highest  $I_p$  ramp rate (0.36 MA/s) where  $l_i \simeq 0.62$ ; this case is not present in the JET-C database. In addition, the measured power threshold  $P_{thr}$  during  $I_p$  ramp up was similar to that obtained in  $I_p$  flat top conditions [7], and lower by  $\sim 30\%$  than in JET-C and than the scaling law prediction  $P_{thr,08}$  [12]. In most discharges no strong W accumulation was observed. However, in some low density cases ( $n_e/n_e^{Gw} \sim 0.2$ ) during the early phase of the  $I_p$  RU strong core radiation due to W influx led to hollow  $T_e$  profiles [13]. These results will be discussed more extensively in Section 6.

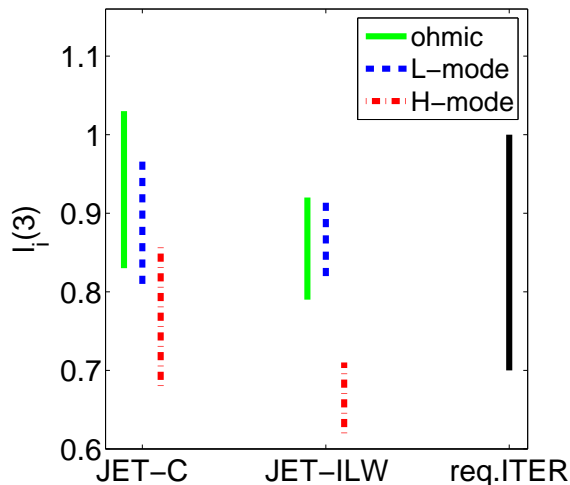


**Figure 2.**  $l_i$  ranges obtained at the end of the  $I_p$  RU in JET-C and JET-ILW, and the acceptable  $l_i$  range for ITER.

### 3. Modelling

Both interpretative and predictive modelling has been performed for a few representative discharges in JET-C and JET-ILW, both with ohmic and H-mode  $I_p$  RU. In the predictive modelling the evolution of  $T_e$  and  $T_i$  is evolved, using experimental data for  $n_e$  and  $Z_{eff}$ . The modelling was done with the CRONOS suite of codes [8]. CRONOS does not use a free-boundary equilibrium solver; however, it can handle time-varying boundaries, e.g. expanding plasma volume and X-point formation, which is sufficient for the present analysis. Sawteeth are taken into account in the modelling; the Porcelli model is used to describe the sawtooth crash [14]. For the predictive modelling the semi-empirical Bohm-gyroBohm transport model is used (L-mode version, [15]), up to the edge in the ohmic and L-mode phases, and up to the top of the pedestal ( $\rho \simeq 0.95$ ) in the H-mode phase, with experimental edge  $T_e$  (50-100 eV) and pedestal height, respectively, as boundary condition. In the past this model has proven to give good reproductions of

**Table 1.** Overview of JET-ILW and JET-C (the latter in italics) ITER like  $I_p$  RU experiments. The quoted values are those obtained at the end of the current rise phase.

dis-charge	$dI_p/dt$ [MA/s]	scenario	injected power [MW]	heating location	$T_e(0)$ [keV]	$\langle n_e \rangle$ [ $10^{19} \text{m}^{-3}$ ]	$Z_{\text{eff}}$	$l_i(3)$
83014	0.28	ohmic	0		1.72	4.8	1.24	0.84
83194	0.28	ohmic	0		1.78	7.4	1.16	0.89
83223	0.28	ohmic	0		1.56	8.2	1.15	0.92
83225	0.36	ohmic	0		1.71	7.18	1.12	0.83
83451	0.5	ohmic	0		1.65	8.82	1.04	0.79
ILW 83224	0.28	H-mode	5, NBI	on-axis	2.71	5.75	1.25	0.69
83444	0.28	H-mode	5, NBI	on-axis	2.0	5.57	1.09	0.70
83445	0.28	H-mode	5, NBI	off-axis	1.84	5.83	1.06	0.68
83446	0.28	H-mode	5, NBI	on-axis	2.9	3.55	1.09	0.69
83447	0.28	H-mode	5, NBI	on-axis	2.5	6.5	1.07	0.72
83449	0.28	L-mode	1.5, RF	on-axis	2.7	5.5	1.10	0.82
83450	0.28	L-mode	2.8, RF	on-axis	1.84	5.6	1.06	0.82
83226	0.36	H-mode	5, NBI	on-axis	2.5	5.73	1.18	0.62
<i>72465</i>	0.19	ohmic	0		2.1	1.5	1.5	1.03
<i>72467</i>	0.28	ohmic	0		2.1	1.5	1.5	0.96
<i>72504</i>	0.28	ohmic	0		1.8	2.3	1.4	0.95
<i>72514</i>	0.28	ohmic	0		2.1	1.5	1.5	0.95
<i>72460</i>	0.36	ohmic	0		2.4	1.1	1.5	0.83
<i>72464</i>	0.36	ohmic	0		2.0	1.6	1.6	0.83
C <i>72505</i>	0.28	L-mode	3, RF	off-axis	3.2	1.6	2.2	0.97
<i>72507</i>	0.28	L-mode	3, RF	on-axis	5.6	1.8	1.8	0.81
<i>72506</i>	0.28	L-mode	6, RF	on-axis	4.5	1.8	2.8	0.86
<i>72509</i>	0.28	L-mode	5, RF	on-axis	6.8	1.8	2.4	0.76
<i>72508</i>	0.28	L-mode	2.2, LHCD	on-axis	4.1	1.4	1.8	0.82
<i>72516</i>	0.28	L-mode	4, NBI	on-axis	3.6	1.9	1.7	0.87
<i>72511</i>	0.28	H-mode	7, NBI	on-axis	4.9	2.1	1.5	0.73
<i>72512</i>	0.28	H-mode	9.8, NBI	on-axis	5.0	2.0	1.6	0.68
<i>72517</i>	0.19	L-mode	5.5, NBI	on-axis	3.8	1.8	2.0	0.83

the  $I_p$  RU phase in JET [4]. It should be noted that first principles models like GLF23 do not reproduce well the ohmic and L-mode  $I_p$  RU [4].

## 4. Comparison of $I_p$ RU in JET-C and JET-ILW

### 4.1. Initial phase after plasma breakdown

The much lower recycling with the ILW requires break-down at higher pre-fill pressures and additional fuelling to maintain the density after break-down. This complicates low voltage break-down in JET-ILW [16]. Within the limited time allocated to the ITER-like  $I_p$  RU experiments in JET-ILW so far, there was no time to explore reduced break-down voltage. The more aggressive break-down causes a faster initial  $I_p$  rise, induces  $n=1$  MHD, hence anomalous inward current and heat transport. Therefore, within 0.5 s after break-down a more peaked  $T_e$  and higher  $l_i$  are observed in JET-ILW discharges, compared to JET-C discharges, see Figures 3,4. Low voltage breakdown with the ILW was successfully optimized after the experiments reported here.

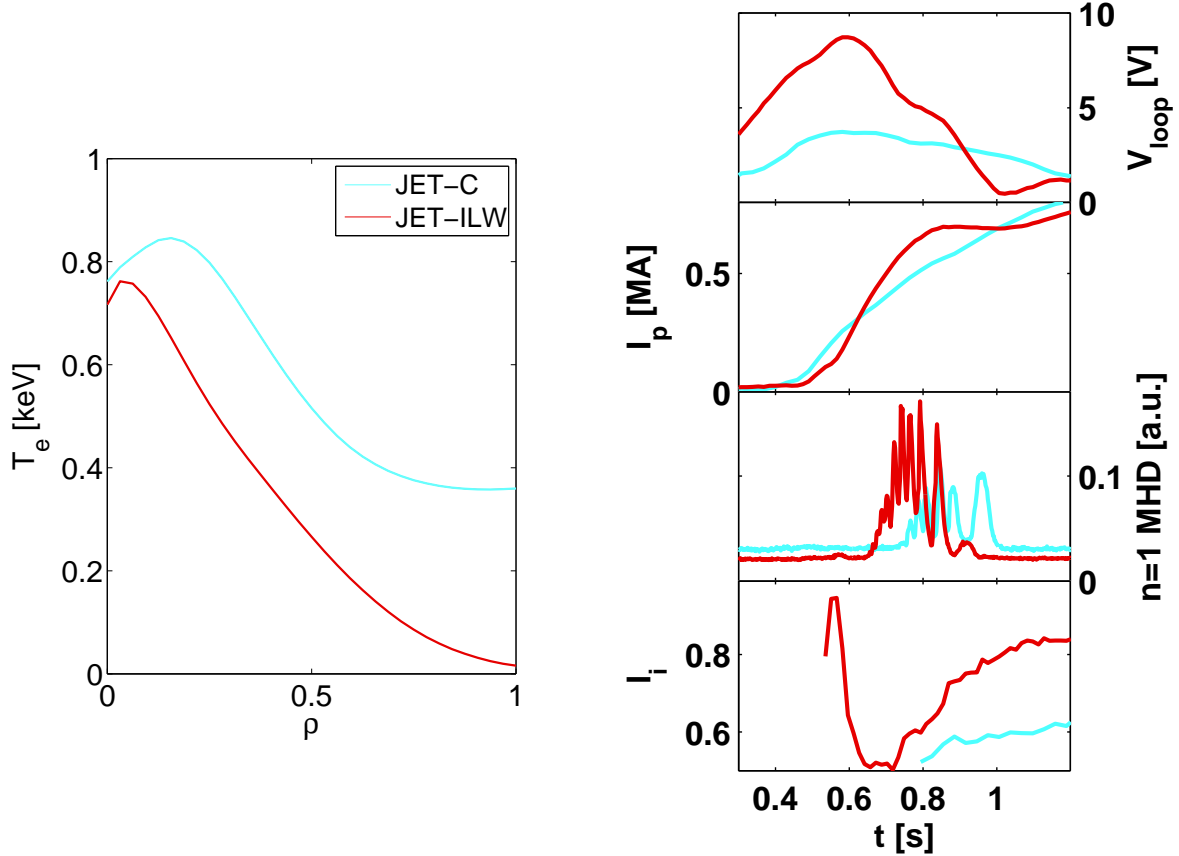


**Figure 3.**  $T_e$  profiles from Michelson interferometer (ECE) at 1.4 s ( $\sim 1$  s after break-down) for the pulses of Fig.1.

**Figure 4.** Comparison of initial phase of ohmic  $I_p$  RU in JET-C (JPN 72723, light cyan) vs. JET-ILW (JPN 83223, dark red): from top to bottom  $V_{loop}$ ,  $I_p$ ,  $n = 1$  MHD signal, and  $l_i$ .

## 4.2. Ohmic RU

Generally, comparing JET-ILW with JET-C pulses with the same  $I_p$  ramp rate, a good match in  $l_i$  and  $T_e(0)$  was observed. Yet there are some differences. The main difference is that  $Z_{\text{eff}}$  is reduced in JET-ILW [17]. For this reason the current diffusion, as measured by  $l_i$ , is slower in JET-ILW compared to JET-C. This compensates for the faster  $l_i$  evolution immediately after BD; consequently after  $\simeq 5$  s  $l_i$  and  $T_e$  peaking (defined as  $T_e(0)/\langle T_e \rangle$ ) are the same in JET-ILW and JET-C, see Fig.1. There is a slight reduction in flux consumption in JET-ILW: the effect of lower  $Z_{\text{eff}}$  is only partially balanced by the slightly lower  $\langle T_e \rangle$  in the JET-ILW pulses. The modelled current diffusion in the first 3 seconds is hampered by the poorly defined initial conditions and the poor quality of the experimental  $T_e$  data in this phase, both from ECE and LIDAR; after this phase the experimentally observed current diffusion is well described by the modelled current diffusion, see Fig.1.

## 4.3. H-mode RU

In JET-ILW the L-H threshold ( $P_{\text{thr}}$ ) is reduced compared to JET-C and significantly below the scaling law prediction ( $P_{\text{thr}08}$ ) in the density range where the scaling law prediction is normally valid; we will not further discuss the possible cause of this here, the reader is referred to [12]. Unfortunately the limited experimental time available did not allow us to increase the NB power above the JET-C  $P_{\text{thr}}$  during  $I_p$  RU. Therefore no good match with JET-C H-mode  $I_p$  RU cases could be obtained. In the following we will compare the JET-ILW H-mode  $I_p$  RU case (JPN 83446) with two JET-C pulses: (i) one H-mode with  $\sim$  double input power (JPN 72512), and (ii) one L-mode with similar input power (JPN 72516), see Fig.5.

In order to sufficiently screen W influx into the plasma core [18], a high gas puff rate of typically  $5 \cdot 10^{21} \text{ s}^{-1}$  is applied during H-mode in JET-ILW, whereas in the JET-C cases the gas puff rate reduced to 0 during H-mode (fuelling by NBI only). This leads to an increase in  $n_e$  during H-mode JET-ILW  $I_p$  RU by more than a factor of 2. Because of the higher  $n_e$ ,  $T_e$  is lower in the JET-ILW case, even lower than in the JET-C L-mode case, see Fig.5c,d,m,n. There is no significant difference in  $T_e$  peaking, see Fig.5e,o. The  $l_i$  reduction achieved with H-mode is the same in JET-ILW and JET-C, although only half the power was applied in the JET-ILW case, see Fig.5h. Like in the ohmic case,  $Z_{\text{eff}}$  is much lower in JET-ILW. The combined effect of lower  $Z_{\text{eff}}$  and lower  $\langle T_e \rangle$  is that the flux consumption in the JET-ILW H-mode  $I_p$  RU case is slightly higher than in JET-C H-mode  $I_p$  RU, and lower than in JET-C L-mode  $I_p$  RU, see Fig.5i,s. The dominant player here is  $Z_{\text{eff}}$ ; note that the difference in  $Z_{\text{eff}}$  between JET-ILW ( $\simeq 1.1$ ) and JET-C ( $\simeq 2.0$ ) is  $\sim 3$  times larger than the combined error bar on both  $Z_{\text{eff}}$  values of  $\simeq 10\%$ . Modelling shows that the effect of replacing  $Z_{\text{eff}}$  in the JET-ILW pulse with the JET-C  $Z_{\text{eff}}$ , keeping all other experimental data fixed, is that the flux consumption increases to the L-mode JET-C case, and also that  $l_i$  increases significantly, see the dashed black curves in Fig.5r,s.



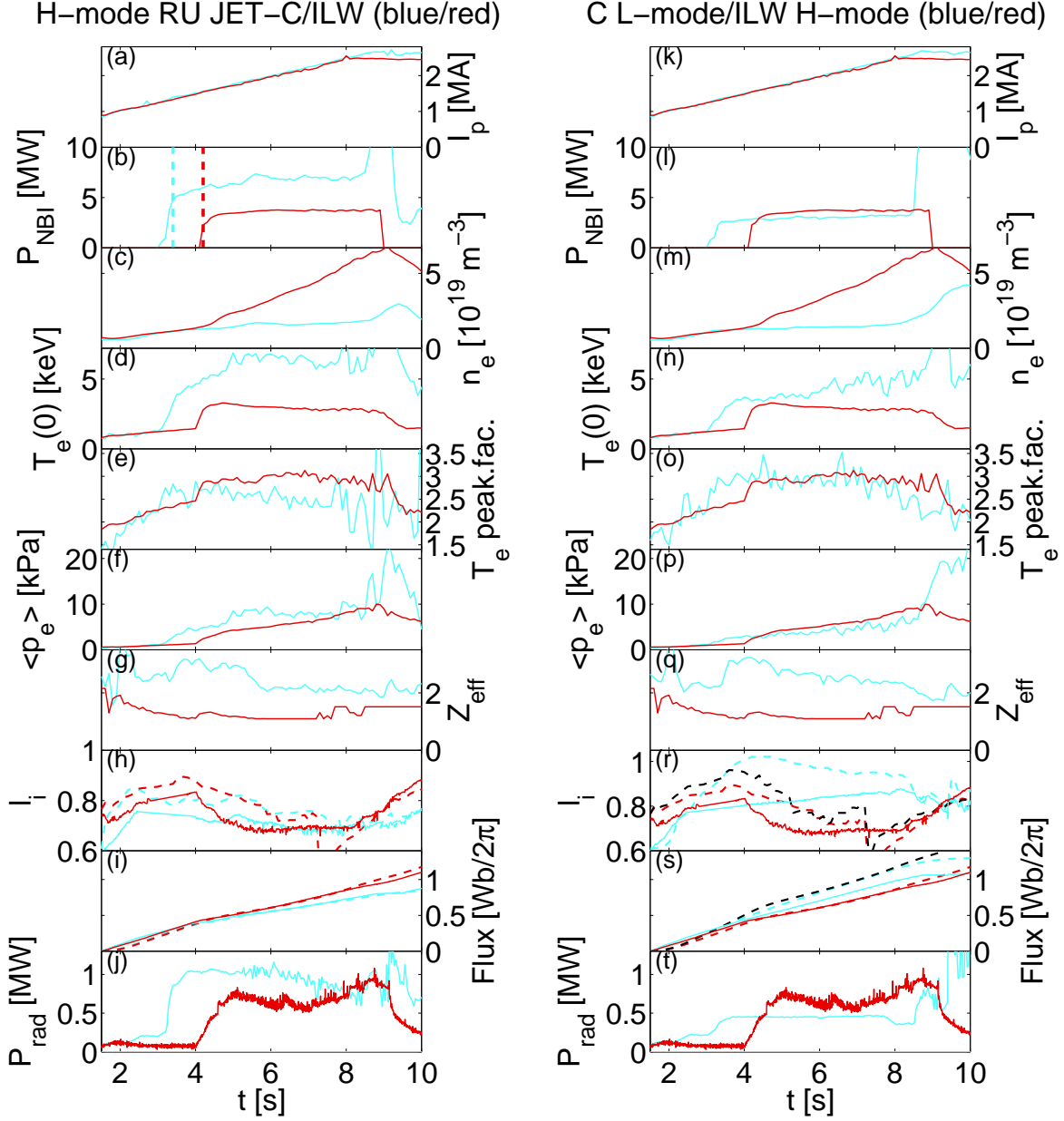


**Figure 5.** Experimental time traces of  $I_p$ ,  $P_{\text{NBI}}$ , line averaged  $n_e$ ,  $T_e(0)$ ,  $T_e$  peaking,  $\langle p_e \rangle$ ,  $Z_{\text{eff}}$ ,  $l_i$ , flux consumption and total radiation for heated  $I_p$  RU. Left JET-ILW H-mode (JPN 83446, dark red) is compared with JET-C H-mode (JPN 72512, light cyan); the right hand panels compare the same JET-ILW H-mode pulse with JET-C L-mode (JPN 72516, blue). The vertical dashed lines in panel (b) indicate the time of the L-H transition. The dashed lines of  $l_i$  and flux consumption are from interpretative modelling. The dashed black curves in the right hand panels of  $l_i$  and flux consumption show the effect of  $Z_{\text{eff}}$ : these curves are the result of interpretative modelling of JPN 83446 ( $Z_{\text{eff}} \sim 1.1$ ), however assuming  $Z_{\text{eff}} \sim 2.0$  as in JPN 72516 (see text).

After the L-H transition, both in JET-C and JET-ILW, the plasma enters ELMy H-mode. However, the ELM characteristics are different in the two cases. In JET-ILW pulses, after a short initial phase with small ELMs at high frequency, regular type-I

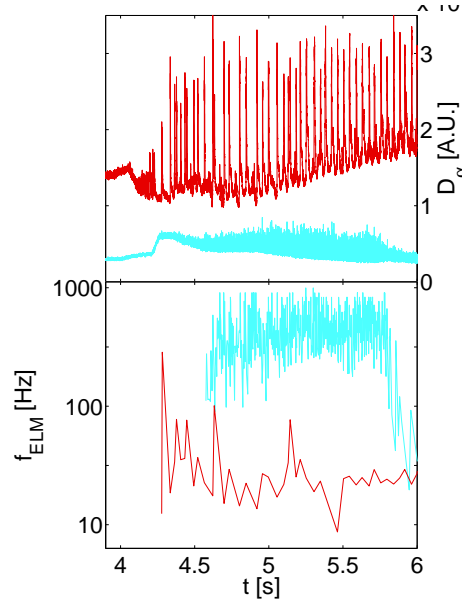


**Figure 6.**  $D_\alpha$  signal (as ELM signature) and ELM frequency during H-mode  $I_p$  RU for JPN 72512 (light cyan, JET-C) and 83224 (dark red, JET-ILW). Note that the ELM frequency is plotted on a logarithmic scale.

ELMS set in with ELM frequency ( $f_{\text{ELMs}}$ )  $\sim 20$  Hz. In contrast, in JET-C  $I_p$  RU type-III ELMs are present with  $f_{\text{ELMs}} \sim 300$  Hz, see Fig.6.

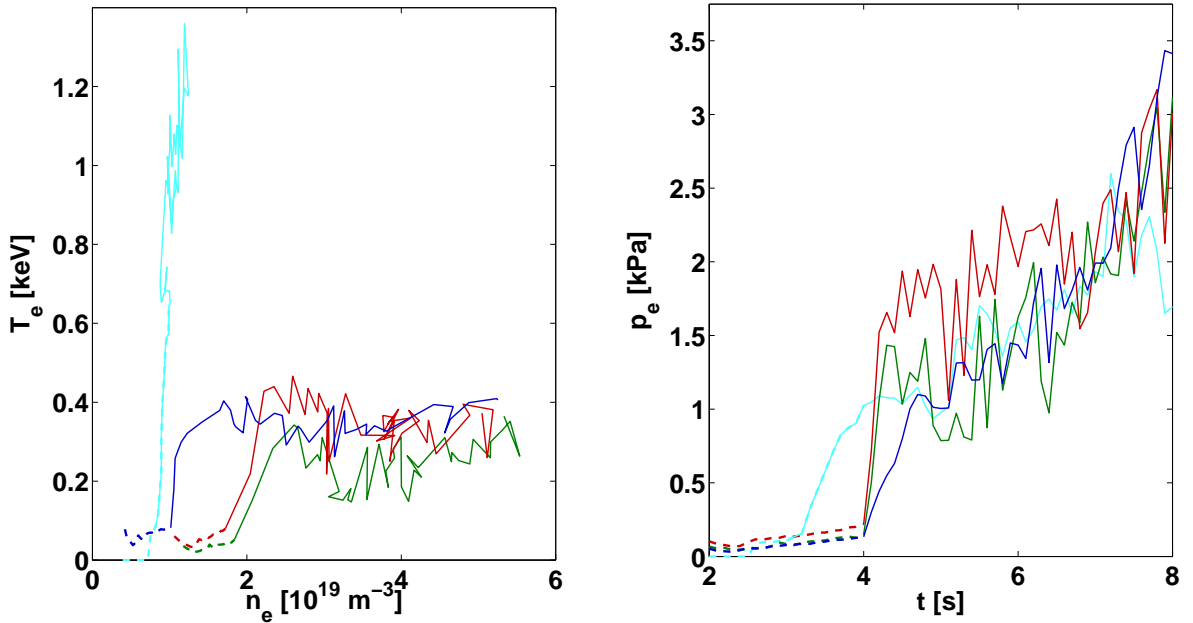


**Figure 7.** Left: Time evolution of  $n_e$  and  $T_e$ , as measured with interferometry and ECE, respectively, at the position of the top of the pedestal for JPN 72512 (JET-C, light cyan) and 83224, 83444, 83446 (JET-ILW, dark green, red, blue), until the end of the  $I_p$  RU at 8 s. The dotted lines indicate the L-mode phase.

Right:  $p_e$  at the top of the pedestal as function of time for the same discharges, with the same colour coding.

Also the pedestal  $T_e$  and  $n_e$  evolution during H-mode  $I_p$  RU in JET-ILW is different from the evolution in JET-C. Due to the stronger gas puff in the JET-ILW case, as reported in the previous section, at the top of the pedestal  $n_e$  is much higher (and increases during the  $I_p$  RU), and  $T_e$  (and  $T_i$ , not shown here) is much lower, see Fig.7a. As a consequence,  $p_e$  at the top of the pedestal is on average the same in JET-ILW as compared to JET-C, see Fig.7b. The same difference is observed during the flat-top [18].

#### 4.4. Thermal transport

Predictive modelling has been performed for a few representative discharges in JET-C and JET-ILW, both with ohmic and H-mode  $I_p$  RU. Time traces of  $T_e(0)$ ,  $q(0)$  and the IPB98 H-mode factor ( $H_{IPB98}$ , [19]) are given in Fig.8, showing good agreement between experiment and modelling results. In Fig.9 the measured and modelled  $T_e$  profiles are compared, both halfway and at the end of the  $I_p$  RU, both for the ohmic and H-mode case. The fact that the modelling is equally satisfactory for JET-C and JET-ILW indicates that there is no fundamental difference in the thermal transport, apart from the different pedestal evolution (where higher  $n_e$  compensates for lower  $T_e$  in JET-ILW) discussed before.

### 5. $l_i$ control and flux consumption reduction in $I_p$ RU and RD

Control of  $l_i$  and limitation of flux consumption during  $I_p$  RU and RD is crucial for ITER operation. In Fig.10 we show three experimental results, supported with data from interpretative modelling:

- $l_i$  during  $I_p$  RU can be controlled and flux consumption reduced by early transition to H-mode, see Fig.10a.
- Similarly sustained H-mode during  $I_p$  RD keeps  $l_i$  and flux consumption low, see Fig.10b.
- In fast ohmic  $I_p$  RD elongation reduction prevents uncontrolled rise of  $l_i$ , see Fig.10c. This is important for ITER when in an emergency case fast current termination is needed and additional heating is unavailable. ITER modelling has shown that this concept indeed is a viable option for ITER [20].

In [2] feedback control on input power was used to demonstrate active control of  $l_i$ ; this was not repeated for JET-ILW  $I_p$  RU discharges.

## 6. Role of W in JET-ILW $I_p$ RU

### 6.1. Experimental observations

The amount of W sputtering from the divertor plates is mainly determined by the divertor temperature ( $T_{e,div}$ ). Langmuir probe measurements show that the inter-ELM

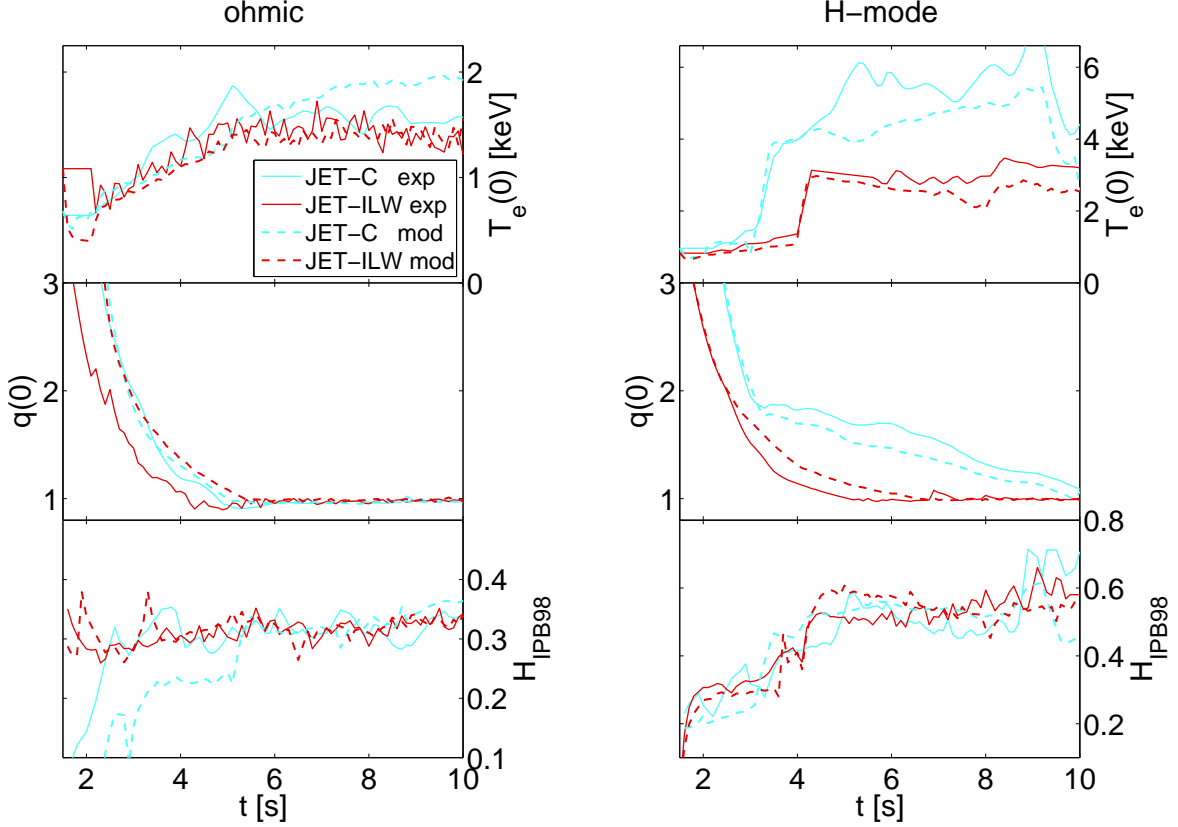


**Figure 8.** Comparison of  $T_e(0)$ ,  $q(0)$  and  $H_{IPB98}$  from experiment (full lines) and from predictive modelling using the Bohm-gyroBohm model (dashed lines), for ohmic (left) and H-mode  $I_p$  RU for JET-C (light cyan) and JET-ILW (dark red). Data from JPN 72723 (ohmic, JET-C), 72512 (H-mode, JET-C), 83223 (ohmic, JET-ILW) and 83224 (H-mode, JET-ILW).

$T_{e,div}$  during H-mode  $I_p$  RU in the experiments under consideration is similar to  $T_{e,div}$  during ohmic  $I_p$  RU,  $\sim 5$  eV. This low  $T_{e,div}$  during H-mode  $I_p$  RU is caused by the strong applied fuelling. However,  $T_{e,div}$  in H-mode  $I_p$  RU during ELMs is much higher ( $\sim 100$  eV). This causes transiently strongly increased W influx in JET-ILW H-mode  $I_p$  RU [21], and hence enhanced core radiation compared to the ohmic phase, see lowest panels of Fig.5. Tomographic reconstruction of SXR emissivity shows that the core radiation is strongly peaked during H-mode  $I_p$  RU, with central value a factor  $\simeq 30$  higher than in an ohmic pulse, see Fig.11. However, the sawteeth, when present, periodically suppress the central peaking.

It is estimated that  $>\simeq 90\%$  of the core SXR emission in JET-ILW discharges comes from W radiation (the remaining fraction mainly comes from Ni) [22]. Using this assumption, the local W concentration  $n_W/n_e$  can be calculated from the local  $T_e$ ,  $n_e$  and SXR emissivity [23]. The SXR signal in ohmic pulses is too low for this W density calculation, hence in the following only the H-mode pulses are analyzed. The left hand panels of Fig.12 show time traces of SXR radiation and calculated W concentration at various radii for JPN 83224, showing the effect of a sawtooth crash on the central W density. The right hand panels of Fig.12 show profiles of SXR radiation and  $n_W/n_e$

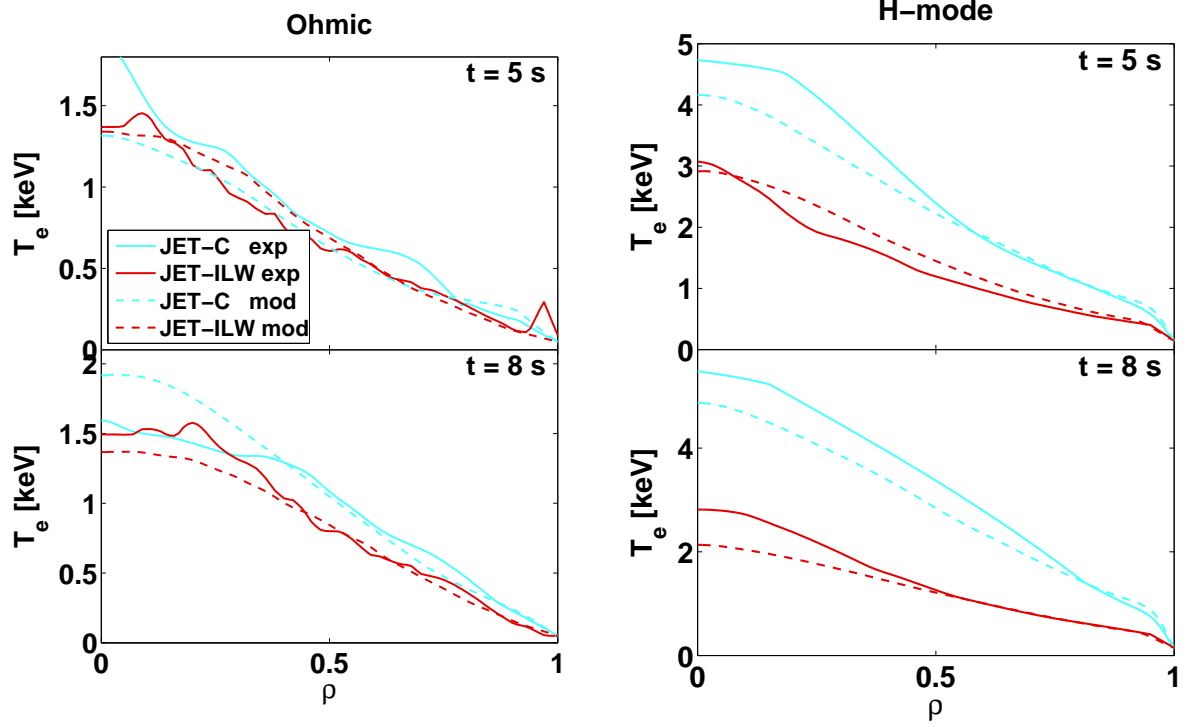


**Figure 9.** Comparison of  $T_e$  profiles halfway (at 5 s) and at the end of the  $I_p$  RU (at 8 s) from experiment (full lines) and from predictive modelling using the Bohm-gyroBohm model (dashed lines), for ohmic (left) and H-mode  $I_p$  RU for JET-C (light cyan) and JET-ILW (dark red). Same colour coding and pulses as Fig.8.

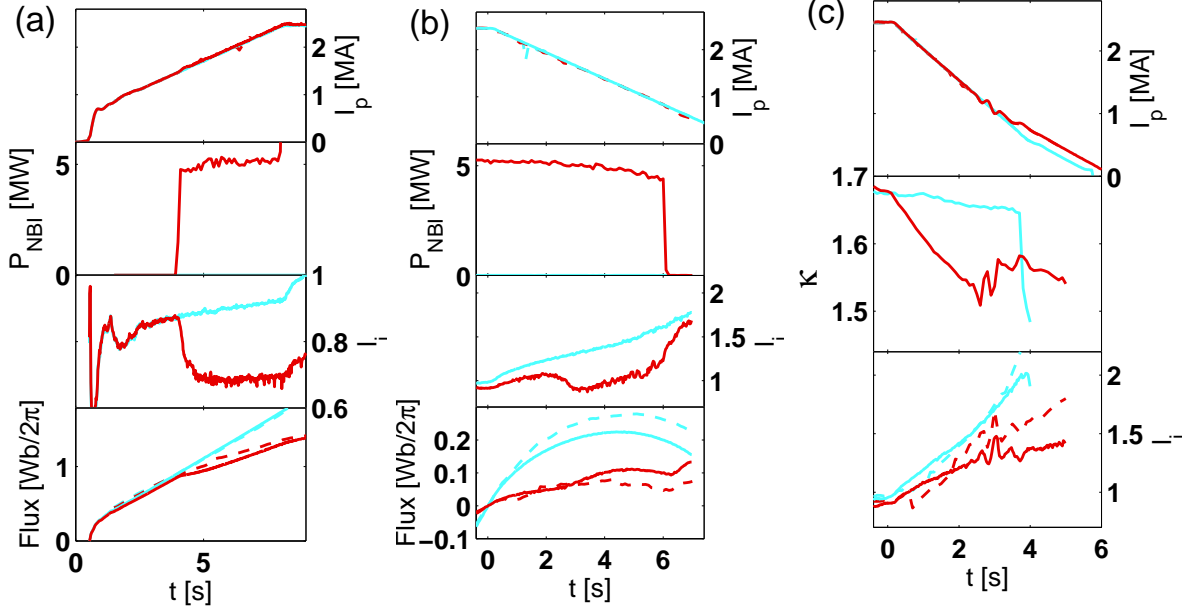


**Figure 10.** *a,b:* Effect of H-mode during  $I_p$  RU (*a*) and RD (*b*) on  $l_i$  and flux consumption. *a:* JPN 83223/83224 (light cyan/dark red); *b:* JPN 83224/83225 (light cyan/dark red); *c:* Effect of fast elongation reduction on  $l_i$  during ohmic  $I_p$  RD: JPN 83449 (light cyan) and 83447 (dark red). In panels *b* and *c* time 0 indicates start of  $I_p$  RD. Dashed lines are interpretative modelling results.

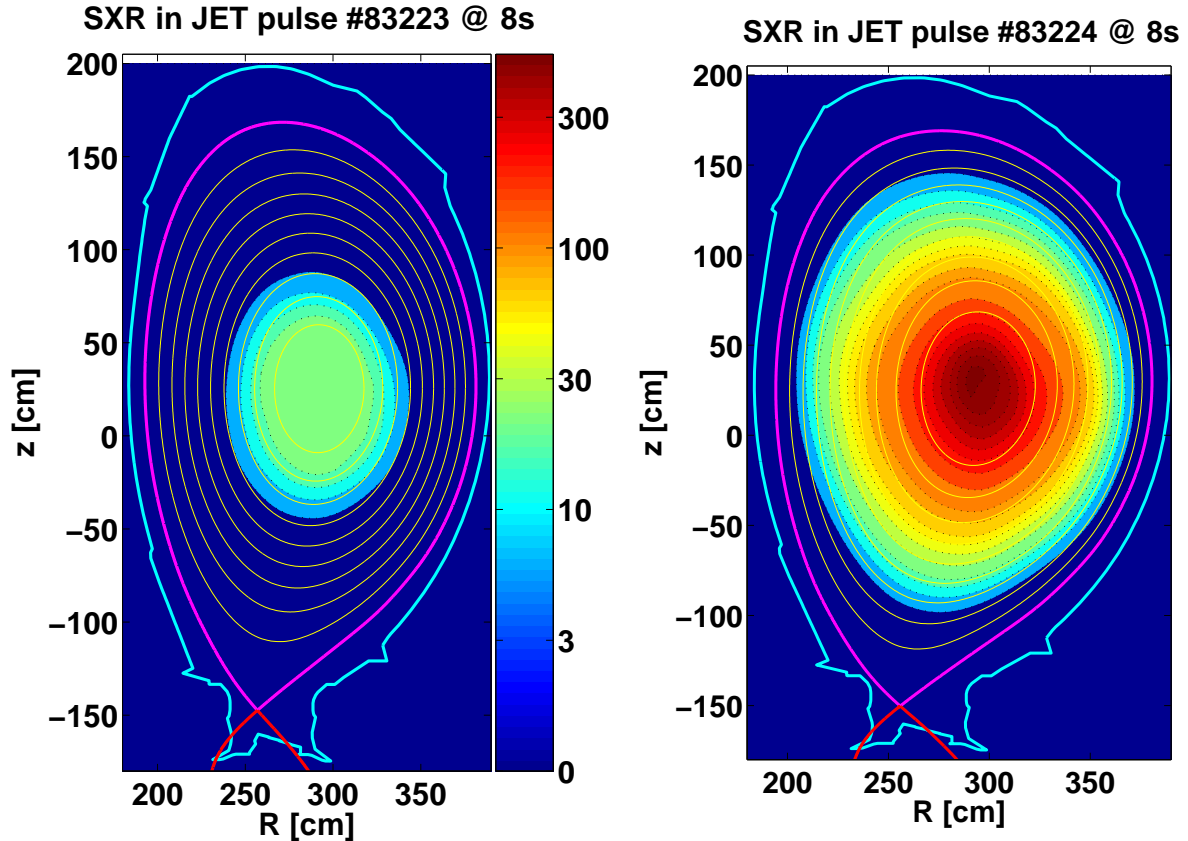


**Figure 11.** Tomographic reconstruction of SXR emissivity at the end of the ramp-up for a JET-ILW ohmic (JPN 83223, left) and H-mode (83224, right) case. The JET vessel (cyan), LCF (magenta) and a number of flux surfaces (yellow) are also shown. The shown color bar is valid for both plots; the unit is  $\text{kW}/\text{m}^3$ . Note that the  $^{10}\log$  of the emissivity is plotted. The emissivity in the H-mode case is much more peaked, and is a factor  $\sim 30$  higher in the centre, compared to the ohmic case.

before and after sawtooth crashes.

It should be noted that the W density can also be determined via JETTO/SANCO [24] impurity transport simulations, where the W influx and W transport coefficients are adjusted iteratively such that the predicted SXR emission matches the measured line integrated emission from three SXR cameras. It has been shown that this method yields similar  $n_W$  profiles [25].

In a few cases a so-called W-event occurred: a sudden influx of W, causing increased core radiation and thus increased central  $n_W/n_e$ ; an example of this is shown in Fig.13 (W-event at 5.5 s). In such cases the radiation temporarily becomes the dominant term in the local power balance in the centre of the plasma, thus leading to a net energy sink in the centre. This in turn leads to a reduction of core  $T_e$ , and finally to a hollow  $T_e$  profile. Sawteeth disappear, as well as the sawtooth induced W removal from the core, leading to an even more peaked W profile. After such an event, the plasma remains in a stable non-sawtooth regime with peaked W profile and hollow  $T_e$  profile, see Fig.14 (and the hollow  $T_e$  profile shown in Fig.16). The  $l_i$  evolution is hardly affected, as the profile changes only occur in a small plasma volume.

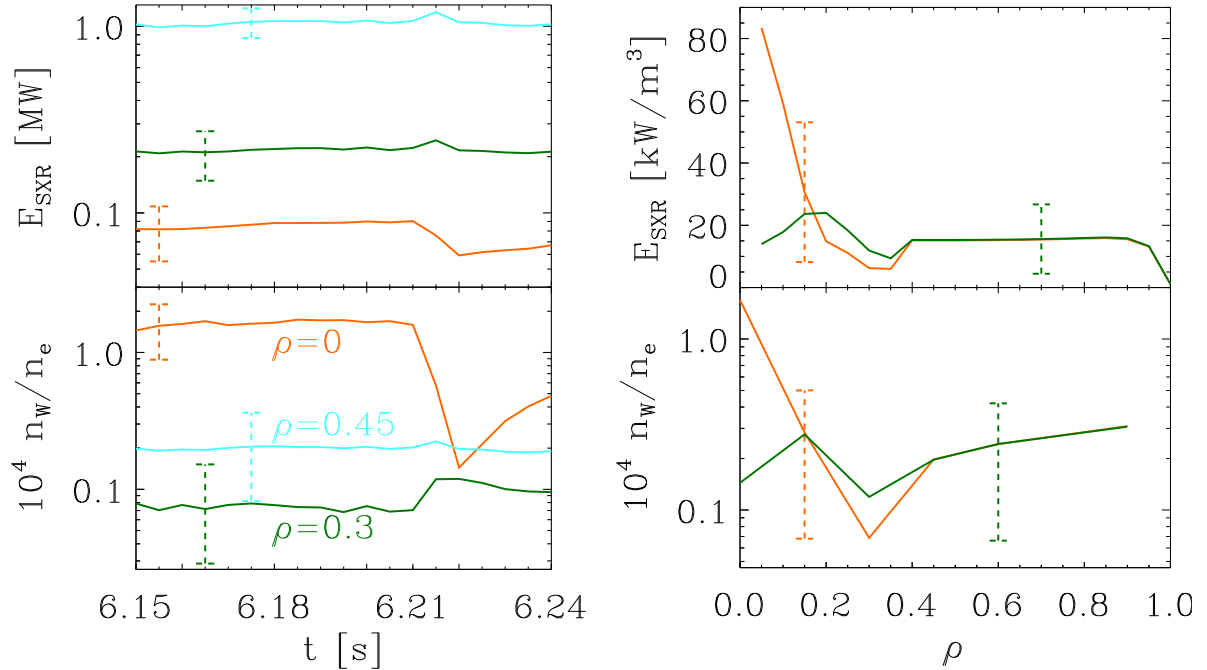


**Figure 12.** SXR radiation (upper panels) and derived W concentration (lower panels) of JPN 83224. Left upper panel: time traces of SXR radiation around a sawtooth collapse: inside separatrix (light cyan), inside  $\rho = 0.4$  (dark green), inside  $\rho = 0.15$  (orange). Left lower panel: W concentration at  $\rho = 0, 0.3, 0.45$  (orange, dark green, light cyan). Right panels: profiles of SXR emissivity (upper) and W profiles (lower) just before (orange) and just after (dark green) sawtooth crash. Typical error bars are indicated.

## 6.2. Predictive modelling

Predictive modelling was performed with CRONOS to assess the effect of W radiation on the discharge evolution, and more specifically to assess the critical  $n_W/n_e$  above which the plasma bifurcates into a non-sawtooth regime with a hollow  $T_e$  profile. This was done both for ohmic  $I_p$  RU (not shown here) and during H-mode  $I_p$  RU, assuming both flat and peaked  $n_W/n_e$  profiles. The  $n_W/n_e$  scan in H-mode was based on JPN 83224, i.e. NBI was switched on at 4 s and the experimental  $n_e$  of this pulse was used. The transport modelling was performed as outlined in Section 3. The W radiation was calculated using atomic physics data from [23]; the predictions of this model only slightly deviate from the simple average ion model [26]. As for  $Z_{\text{eff}}$ , for the reference run without W the experimental line averaged  $Z_{\text{eff}}$  was assumed, independent of radius, with Be as only impurity. Subsequently, increasing  $n_W/n_e$  fractions were added, without changing the Be concentration, thus leading to a modest increase of  $Z_{\text{eff}}$ , but significant increase in core radiation.

A low  $n_W/n_e$  concentration of  $10^{-5}$  was assumed in the ohmic phase, as observed in the experiments; in the H-mode phase higher  $n_W/n_e$  concentrations were assumed, up to  $2 \cdot 10^{-4}$ . When flat  $n_W/n_e$  is assumed, increasing  $n_W/n_e$  from  $10^{-5}$  to  $10^{-4}$  leads to lower  $T_e$  and an enhanced flux consumption; however, the  $l_i$  evolution and  $q$  profile are nearly unchanged, see Fig.15.

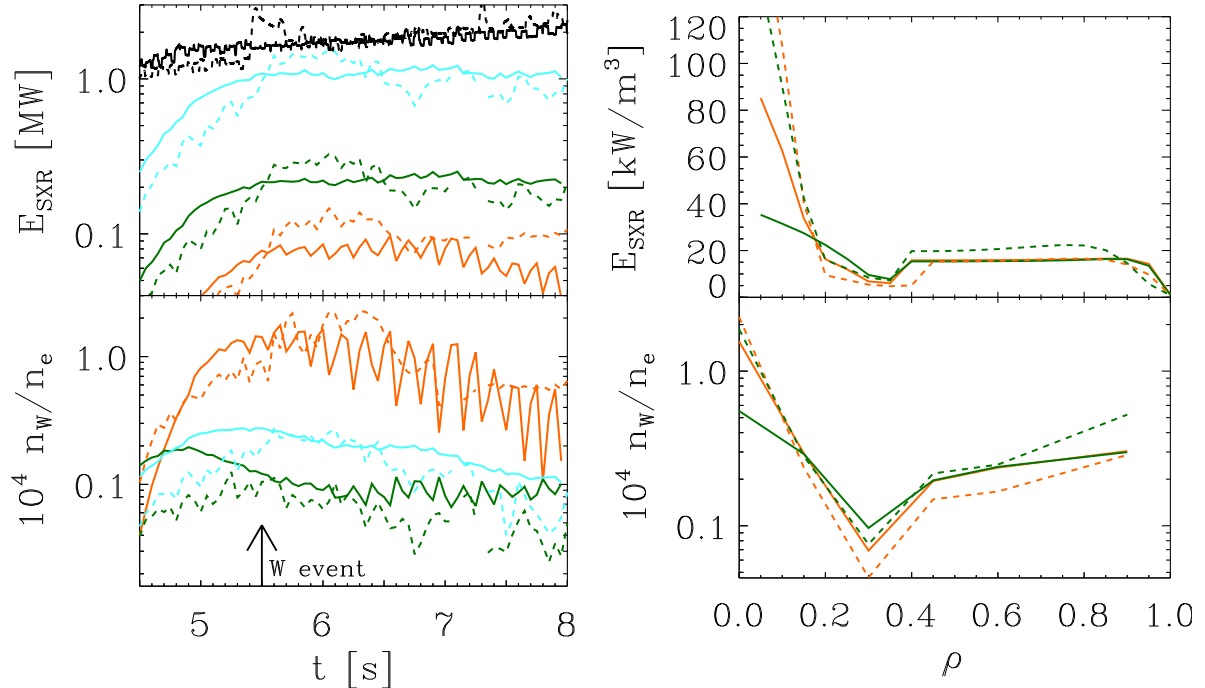


**Figure 13.** Comparison of JPN 83224 (full lines) and 83444 (dashed lines), the latter showing a W event. Left upper panel: time traces of SXR radiation inside  $\rho = 1, 0.4$  and  $0.15$  (light cyan, dark green, orange); in black the total radiated power. Left lower panel:  $n_W/n_e$  at  $\rho = 0, 0.3, 0.45$  (orange, dark green, light cyan). Right panels: profiles of SXR emissivity and W profiles at selected time slices around  $t = 6$  s, showing continuous peaking of radiation and W concentration for JPN 83444, whereas the peaking is interrupted by the sawteeth for JPN 83224.

The behaviour with peaked  $n_W/n_e$  is completely different: here a transition to a non-sawtooth regime with a hollow  $T_e$  profile and reversed magnetic shear is observed above a critical central  $n_W/n_e \sim 10^{-4}$ , see Fig.16. It should be noted that the case with  $n_W/n_e(0) = 10^{-4}$  (green dashed line) is just at the margin: it has a few sawteeth and then has  $q > 1$ . This critical  $n_W/n_e$  for the peaked case agrees very well with the experimental findings as described in the previous subsection, see Fig. 13. The modelling confirms the experimental observation that the  $l_i$  evolution is hardly affected; only with a much higher central  $n_W/n_e$  of order  $10^{-4}$ , one sees a significant reduction of  $l_i$ .

### 6.3. Extrapolation to ITER

In ITER W radiation will be different than in current devices. Because of the higher  $T_e$  in ITER, the W radiation peak will move (far) off axis. An example of this is shown in Fig.17. This will strongly modify the effect of W influx on the discharge evolution. Instead of hollow  $T_e$  and reversed shear, one might expect the opposite, i.e. very peaked  $T_e$  and in extreme cases an effective shrinking of the plasma column.

We have thus modelled the effect of W radiation for an ITER case, under conditions of ohmic, L-mode and H-mode  $I_p$  RU and assuming both flat and peaked  $n_W/n_e$ . Some simulations were post-processed by the FREEBIE code [27] to compute the currents in



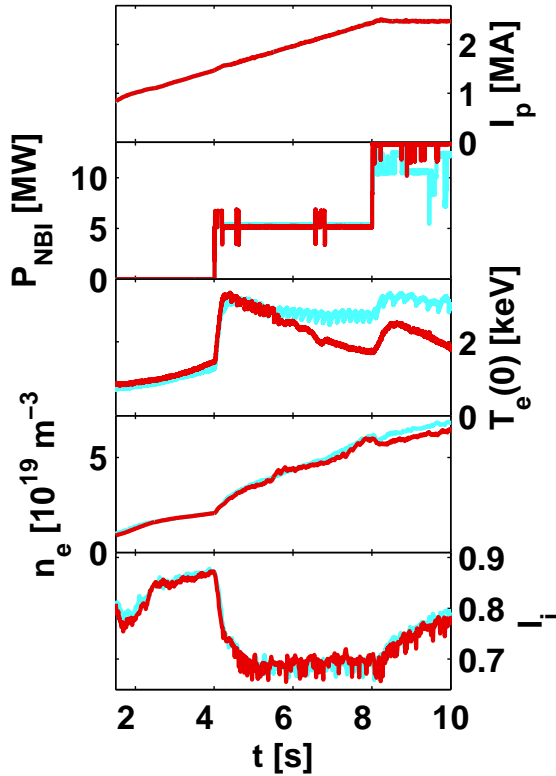


**Figure 14.** Time traces of  $I_p$ ,  $P_{\text{NBI}}$ ,  $T_e(0)$ ,  $\langle n_e \rangle$  and  $l_i$  for JPN 83224 (light cyan) and 83444 (dark red). Although central  $T_e$  is strongly reduced in pulse 83444,  $l_i$  is not affected.

the PF coils, allowing to check that the designed scenario stays within the CS and PF coils operational limits.

Full results of this modelling will be published in a forthcoming paper [28]. Here only a brief summary is given. For the case of flat  $n_W/n_e$  the simulations show that an ohmic  $I_p$  RU in ITER can only tolerate a W concentration of order  $10^{-4}$ . Indeed the effect is a peaking of the  $T_e$  profile, resulting in unacceptably high  $l_i$  up to more than 1.5. Off-axis ECRH can counteract this: when 20 MW of off-axis ECRH power is applied from early in the  $I_p$  RU, the critical W concentration is increased by a factor of  $\simeq 4$ . Because of the low radiation of W at the high core  $T_e$  expected in ITER, a peaked W radiation profile will only occur in case of strongly peaked  $n_W/n_e$ ,  $n_W/n_e(0)/n_W/n_e(\rho = 0.5) > \simeq 5$ . A hollow  $T_e$  profile during the ohmic ITER  $I_p$  RU can be expected only when  $n_W/n_e$  is extremely peaked and  $n_W/n_e \simeq 3 \cdot 10^{-4}$ .

## 7. Conclusions, Discussion and Outlook

Initial JET-ILW ITER-like  $I_p$  RU and RD experiments have allowed gaining useful insight for ITER. Despite changes to the plasma composition in going from JET-C to JET-ILW, the main results obtained in the JET-C experiments are preserved; in

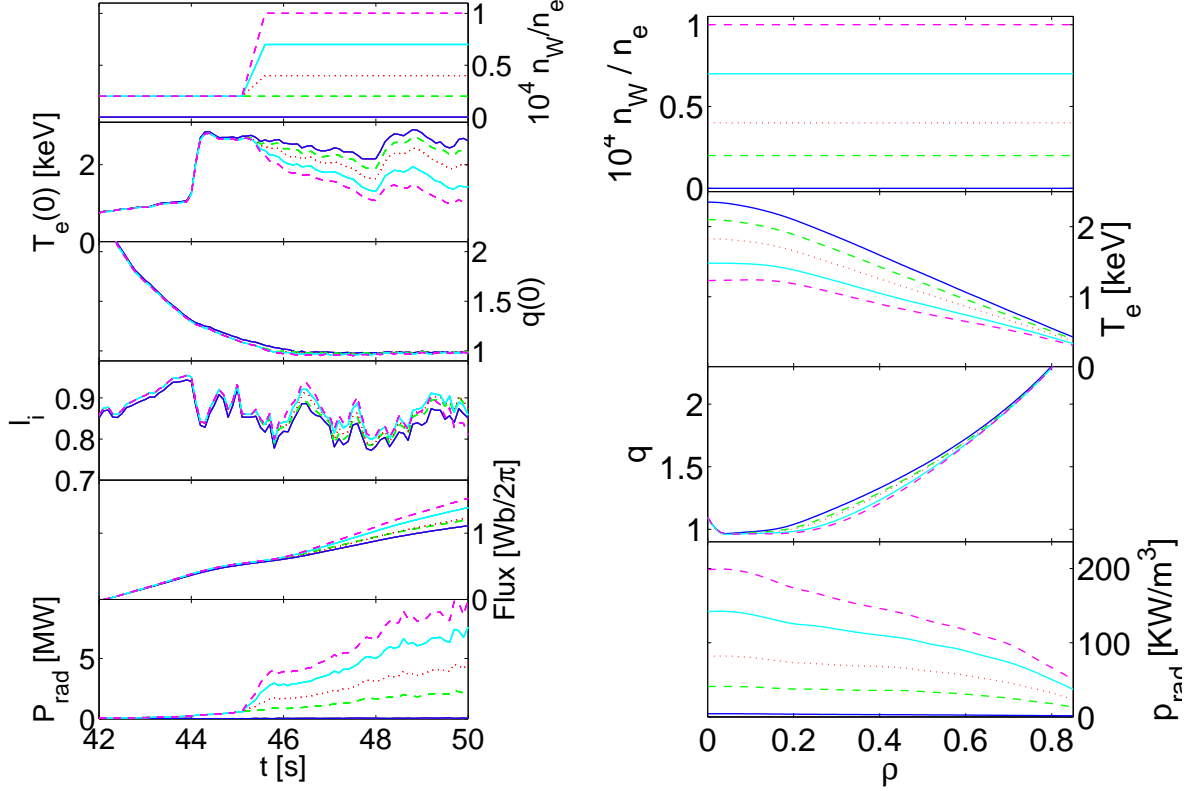


**Figure 15.** Results of predictive modelling of various  $W$  concentrations, based on JPN 83224, assuming flat  $n_W/n_e$ . Left: time traces of  $n_W/n_e$ ,  $T_e(0)$ ,  $q(0)$ ,  $l_i$ , flux consumption and  $P_{\text{rad}}$ . Right: profiles of  $n_W/n_e$ ,  $T_e$ ,  $q$  and  $P_{\text{rad}}$  at the end of  $I_p$  RU (8 s).

particular a similar range in  $l_i$  is achieved.  $Z_{\text{eff}}$  is significantly lower in JET-ILW discharges, compared to JET-C; this leads to a slower current diffusion and slightly lower flux consumption in JET-ILW. As was already seen in JET-C, with H-mode  $I_p$  RU and sustained H-mode far into  $I_p$  RD,  $l_i$  can be kept within acceptable ITER-limits, and strong reduction of flux consumption is obtained.

A new element, and key for ITER, is the role of  $W$  in the discharge evolution. The effect of  $W$  on  $Z_{\text{eff}}$  is small; even when  $n_W/n_e = 10^{-4}$ , its contribution to  $Z_{\text{eff}}$  is only 0.16. However, during H-mode  $I_p$  RU  $n_W/n_e$  can peak strongly, and core  $W$  radiation is in these cases significant. Sawteeth suppress the  $n_W/n_e$  peaking, and keep  $W$  radiation under control. In some cases a sudden extra  $W$  influx leads to enhanced radiation; the plasma then tends to bifurcate into a non-sawtooth regime with hollow  $T_e$  and reversed magnetic shear. Once the plasma has entered such regime, it is hard to recover to the usual (sawtoothing) regime, and similar incidents during the flat-top have shown that this event may eventually lead to a disruption [29]. This also implies that control of  $W$  influx is even more important for advanced scenarios, which are sawtooth free. Indeed, in  $I_p$  RU experiments for the hybrid scenario, which are typically sawtooth-free, there are many cases with strong  $W$  peaking and strongly hollow  $T_e$  profiles [13].

Future JET ITER-like  $I_p$  RU and RD experiments will explore ramp rates different from the standard 0.28 MA/s. Moreover, in order to have a better match with JET-C

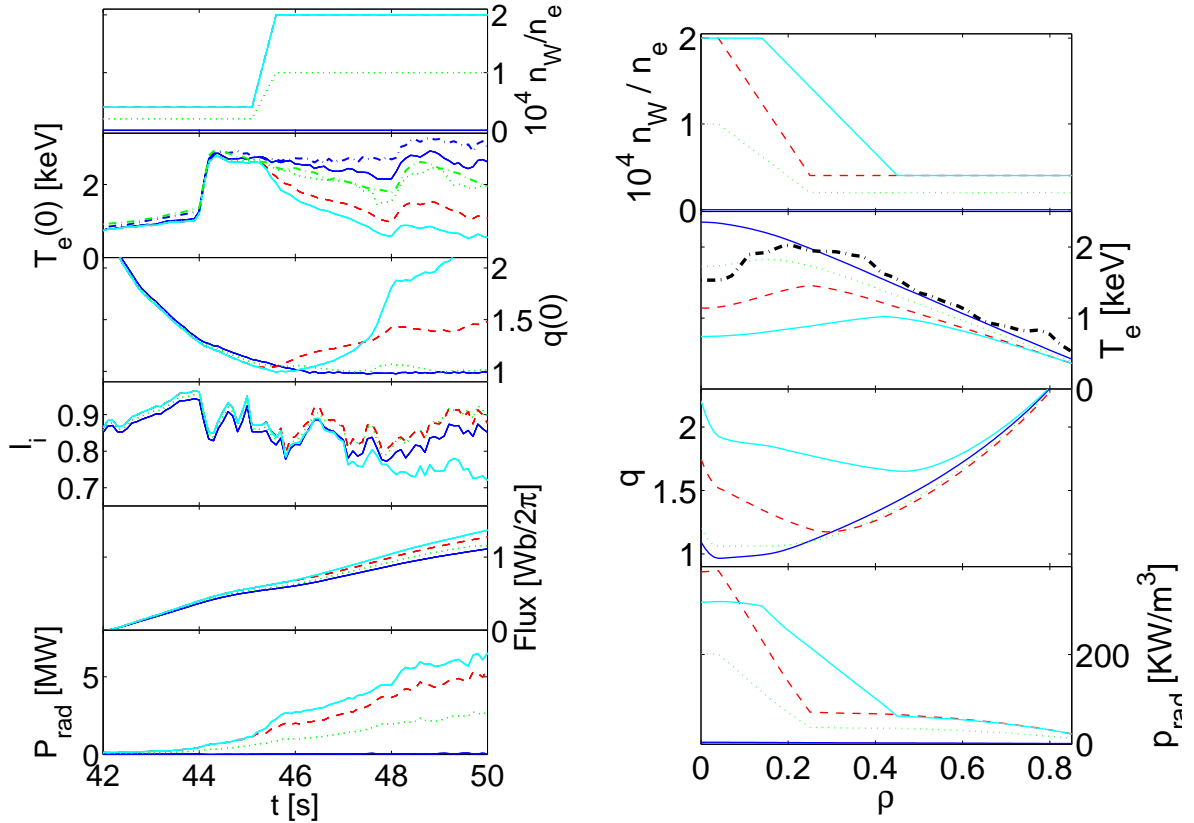


**Figure 16.** Same plots as Fig.15, now assuming peaked  $n_W/n_e$ . For comparison also experimental time traces of  $T_e(0)$  are plotted: blue/green dashed dotted lines for JPN 83224/83444. The measured  $T_e$  profile (from ECE) at 8 s of JPN 83444 is plotted as well (black dashed dotted line), showing a moderate hollowness for JPN 83444, in good agreement with the modelled profile with the same  $n_W/n_e$  (dotted green curve).

experiments, H-mode  $I_p$  RU and RD will be performed at enhanced NBI power.

Predictive modelling has assessed the role of W radiation in the discharge evolution. It was shown that a flat  $n_W/n_e$  is not very harmful to the stability of the discharge, as  $q$  profile and  $l_i$  are not affected. Peaked  $n_W/n_e$  was shown to lead to a non-sawtooth regime with hollow  $T_e$  and reversed magnetic shear above a critical central value of  $\simeq 10^{-4}$ , in very good agreement with the experimental findings.

To avoid deleterious W peaking in H-mode ITER pulses, it might be essential to have a sawtooth plasma or to apply significant central (electron) heating. The latter has proven to be an effective tool to enhance turbulent transport and even to reverse the sign of the convective impurity transport in e.g. AUG [30], and may be essential for advanced (sawtooth-free) scenarios. It should be noted that neoclassical inward convection is the most important W transport term when  $n_e$  is peaked [25]. These requirements are likely to put extra constraints on the ITER operational space or the range of plasma operating scenarios that can be used.

For a more realistic assessment of the role of W in the discharge evolution, the assumed  $n_W/n_e$  profiles should be replaced by calculated profiles. For this purpose a simple (semi-empirical) transport model for W would be needed to be built into a

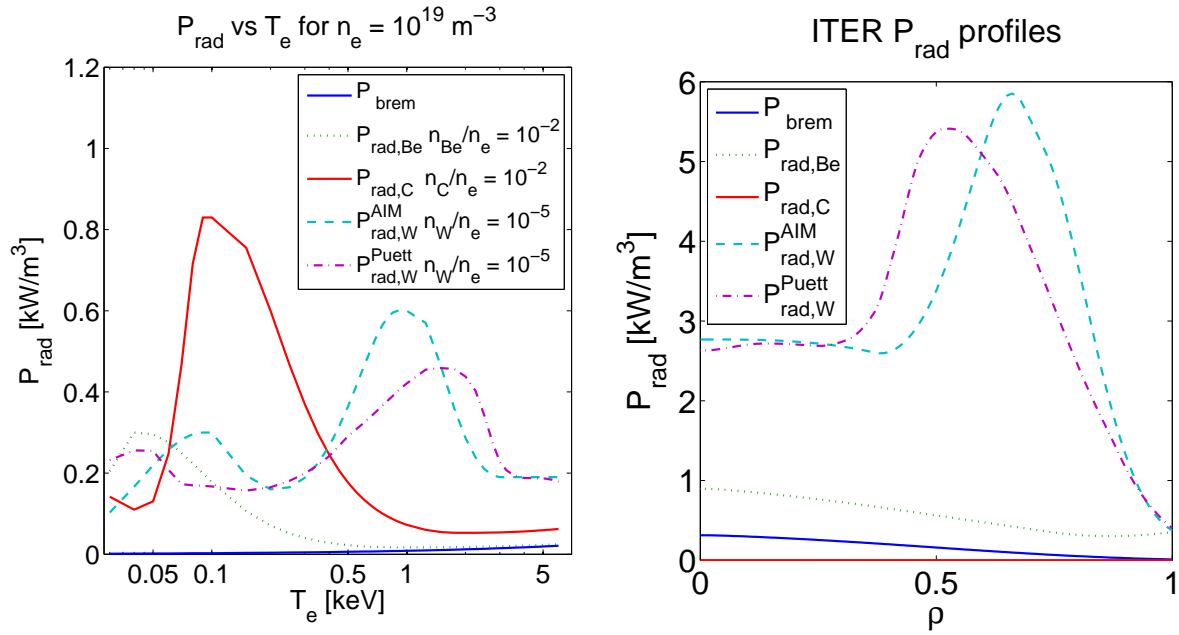


**Figure 17.** Left: radiation per m<sup>3</sup> for Bremsstrahlung and Be, C and W impurities at the given concentrations, as function of T<sub>e</sub>. Right: radial profile of radiation per m<sup>3</sup> for the same impurities, in the last phase of a typical ohmic ITER I<sub>p</sub> RU, showing far off-axis peaking of W radiation. Two profiles are given for the W radiation, based on [26] (labelled AIM) and [23] (labelled Puett). Parameters: I<sub>p</sub> = 10 MA, T<sub>e</sub>(0) = 6 keV, n<sub>e</sub>(0) = 2.5 · 10<sup>19</sup> m<sup>-3</sup>, Z<sub>eff</sub> = 1.8, only impurities assumed are Be with n<sub>Be</sub>/n<sub>e</sub> = 0.06 and W with n<sub>W</sub>/n<sub>e</sub> = 2.3 · 10<sup>-5</sup>.

transport code. It has been shown that core W transport is predominantly neoclassical [25], so a first ansatz could be to take into account only neoclassical W transport.

## References

- [1] N. Holtkamp et al, in Fusion Energy 2008 (Proc. 22nd Int. Conf. Geneva, 2008) (Vienna: IAEA) CD-ROM file [OV/2-1] and <http://www-naweb.iaea.org/naweb/physics/FEC/FEC2008/html/index.htm>
- [2] A.C.C. Sips et al 2009 *Nucl. Fusion* **49** 085015
- [3] I. Nunes et al 38th EPS Conf. on Plasma Physics (Strasbourg, France) 2011, P4.106
- [4] F. Imbeaux et al 2011 *Nucl. Fusion* **51** 083026
- [5] T. Casper et al 2011 *Nucl. Fusion* **51** 013001
- [6] E. Joffrin et al 2014 *Nucl. Fusion* **54** 013011
- [7] G. Calabrò et al, 40th EPS Conf. on Plasma Physics (Espoo, Finland) 2013, O2.106
- [8] J.-F. Artaud et al 2010 *Nucl. Fusion* **50** 043001
- [9] G. De Tommasi et al, 2013 *Fusion Eng. Design* **88** 400
- [10] Y. Martin et al, 2008 *J.Phys.: Conf.Ser.* **123** 012033
- [11] G. De Tommasi et al, 2014 *J. Fusion Energy* **33** 149
- [12] C.F. Maggi et al, 2014 *Nucl. Fusion* **54** 023007
- [13] J. Mailloux et al, 39th EPS Conf. on Plasma Physics (Stockholm, Sweden) 2012, P4.084
- [14] F. Porcelli et al 1996 *Plasma Phys. Control. Fusion* **38** 2163
- [15] M. Erba et al 1998 *Nucl. Fusion* **38** 1013
- [16] P.C. de Vries et al 2013 *Nucl. Fusion* **53** 053003
- [17] S. Brezinsek et al 2013 *Nucl. Fusion* **53** 083023

- [18] M.N.A. Beurskens *et al* 2013 *Plasma Phys. Control. Fusion* **55** 124043
- [19] ITER Physics Basis 1999 *Nucl. Fusion* **39** 2137
- [20] J. Garcia *et al*, submitted to *Nucl. Fusion*
- [21] G.J. van Rooij *et al* 2013 *J. Nucl. Mat.* **438** S42
- [22] Th. Pütterich *et al* 2013 *Plasma Phys. Control. Fusion* **55** 124036
- [23] Th. Pütterich *et al* 2010 *Nucl. Fusion* **50** 025012
- [24] L. Lauro Taroniet *al* 21st EPS Conf. on Contr. Fusion and Plasma Physics (Montpellier, France) 1994, Vol. 1, p.102
- [25] C. Angioni *et al* 2014 *submitted to Nucl. Fusion*
- [26] D. Post. *et al*, *At. Data Nucl. Data Tables* 1977 **20** 397
- [27] Artaud J.-F. *et al*, 39th EPS Conf. on Plasma Physics (Stockholm, Sweden) 2012, P4.023
- [28] Hogeweyj G.M.D. *et al*, to be published in Proc. of the 25th Fusion Energy Conference (FEC 2014), Saint Petersburg, Russia.
- [29] P.C. de Vries *et al* 40th EPS Conf. on Plasma Physics (Espoo, Finland) 2013, P5.166
- [30] R. Neu *et al* 2002 *Plasma Phys. Control. Fusion* **44** 811

## Acknowledgements

This work, supported by the European Communities under the contract of Association between EURATOM/FOM, was carried out within the framework of the European Fusion Programme with financial support from NWO. The views and opinions expressed herein do not necessarily reflect those of the European Commission. This work is supported by NWO-RFBR Centre-of-Excellence on Fusion Physics and Technology (Grant nr. 047.018.002).